Electrochemistry Communications 69 (2016) 55–58

Contents lists available at ScienceDirect

Electrochemistry Communications

journal homepage: www.elsevier.com/locate/elecom

Copper-enriched palladium-copper alloy nanoparticles for effective electrochemical formic acid oxidation

Qi Zhao [a], Juan Wang [a], Xing Huang [b,*], Yuanying Yao [a], Wei Zhang [c], Lidong Shao [a,*]

[a] Shanghai Key Laboratory of Materials Protection and Advanced Materials in Electric Power, Shanghai University of Electric Power, Shanghai 200090, China
[b] Department of Inorganic Chemistry, Fritz-Haber Institute of the Max Planck Society, Faradayweg 4-6, 14195 Berlin, Germany
[c] CIC Energigune, Parque Tecnológico de Álava, Miñano 01510, Bilbao 48011, Spain

ARTICLE INFO

Article history:
Received 29 April 2016
Received in revised form 31 May 2016
Accepted 31 May 2016
Available online 1 June 2016

Keywords:
Formic acid
Copper-enriched
Palladium-copper alloy
Carbon nanotube

ABSTRACT

In this work, Pd-Cu alloy nanoparticles (NPs) with different atomic ratios are prepared on functionalized carbon nanotubes (CNTs) and applied as electrocatalysts for formic acid oxidation. The Cu-enriched Pd-Cu alloy NPs exhibit improved electrocatalytic activity and stability. Functionalized carbon supports are applied as substrates to tune the nanoscale morphologies of the obtained bimetallic phases under appropriate calcination and hydrogenation treatments. Spill-over effect aids a reduction of a high weight loading of Cu in its metallic phase, in turn, these Cu atoms integrate into Pd lattice and isolate Pd neighbouring atoms. Surface analyses show that a certain amount of the isolated Pd remains on the surfaces of Pd-Cu alloy NPs, which is responsible for the enhanced electrocatalytic performance.

1. Introduction

In recent years, formic acid, which represents a new feedstock for fuel cells, has been widely investigated because it is non-toxic and exhibits a low crossover rate through Nafion membranes. Direct formic acid fuel cells (DFAFCs) have favourable oxidation kinetics, low operating temperatures, and high theoretical open-circuit potentials, and they effectively overcome the H_2-storage and transport problems associated with proton-exchange membrane fuel cells (PEMFCs) and the toxicity of the methanol used in direct methanol fuel cells (DMFCs). Thus, they open up a pathway for the development of a new type of portable power [1–3].

Currently, the catalytic materials that are most commonly used as fuel cell anodes are Pt-based alloys [4,5]. However, Pt resources are limited, expensive, and prone to carbon monoxide (CO) poisoning, and thus, the application of Pt catalysts is limited [3,6,7]. Pd and Pt are elements of the same group and have similar characteristics, including face-centred cubic (fcc) crystal structures and similar atomic sizes. Pd-based catalysts are considered to be better electrocatalysts than Pt-based ones because the reaction on the Pd surface follows a direct pathway. Nevertheless, the inferior electrocatalytic stability of Pd catalysts has limited their development [8]. Introducing structural modifications by adding foreign atoms to generate Pd-based alloys has been investigated to enhance the catalytic activity at low overpotentials and increase the stability of Pd-based catalysts. However, the practical application of Pd-based alloys as electrocatalysts for DFAFCs remains challenging. First, Pd and other added metals have been reported to exceed 20–30 wt% [9,10]. Using this amount of metals prohibits the metal dispersion in nanoscale and limits the accessible surface areas during catalysis. Second, the effects of the surface electronic properties and structural stabilities of bimetallic compounds (controlled by bonding patterns) on HCOOH oxidation remain unclear.

Herein, Pd-Cu alloys with various Pd:Cu molar ratios are fabricated on carbon nanotubes (Pd_xCu_y/CNTs) for catalytic studies in HCOOH oxidation. Functionalized CNTs embed nanocrystals of the formed alloy particles and facilitate their nanoscale dispersion during calcination and reduction treatments. The HCOOH oxidation results indicate that Cu-enriched Pd-Cu alloy NPs exhibit enhanced activity and stability relative to the other Pd_xCu_y alloys with lower Cu contents. Furthermore, surface and structural analyses reveal that the surface electronic properties of Cu-enriched Pd-Cu alloy NPs may govern the catalytic pathways.

2. Materials and methods

PR24 low-heat-treated (LHT) CNTs (1 g) were functionalized by oxidation in concentrated HNO_3 (300 mL) for 1 h at 120 °C [11]. Pd_xCu_y/CNTs (where $x:y = 1:0, 3:1, 1:1, 1:3$, or $0:1$) were synthesized as following: in the case of Pd_1Cu_3/CNTs, 31.8 μL of $Pd(NO_3)_2$ (10 wt%, Sigma–Aldrich) solution, 11.2 mg $Cu(NO_3)_2$ (Sigma-Aldrich) were mixed into 20 mL ethanol, followed by adding 50 mg of CNTs to allow coordination with functionalities as anchoring sites. Stirring was maintained at 45 °C throughout the impregnation process until the solution had dried. The

---

* Corresponding authors.
E-mail addresses: xinghuang@fhi-berlin.mpg.de (X. Huang), lidong.shao@shiep.edu.cn (L. Shao).

http://dx.doi.org/10.1016/j.elecom.2016.05.021
1388-2481/

collected powder was calcined in a muffle for 2 h at 250 °C and then annealed in a tube furnace for 2 h at 250 °C under a He/H_2 atmosphere (He, 100 mL/min; H_2, 25 mL/min). The preparation of other samples used a similar method. The atom ratios in terms of real metal weight percentages in the alloy NPs were measured by the inductively coupled plasma atomic emission spectroscopy (ICP): Pd/CNTs (3.25 wt%), Pd_1Cu_3(Pd 3 wt%, Cu 5.25 wt%), Pd_1Cu_1(Pd 2.8 wt%, 1.6 wt%), Pd_3Cu_1(Pd 2.8 wt%, Cu 0.7 wt%). The weight percent of Cu in Cu/CNTs was 3 wt%. X-ray diffraction (XRD) was performed using a Bruker D8 Advance XRD instrument with Cu-Kα radiation. An aberration-corrected JEOL JEM-ARM200CF transmission electron microscope was employed to investigate structural and chemical properties in STEM mode. X-ray photoelectron spectroscopy (XPS) was conducted with a Thermo ESCALAB 250 XPS instrument using a monochromatic Al Kα source (1486.6 eV).

3. Results and discussion

Fig. 1a shows the dispersion of Pd-Cu NPs on the Pd_1Cu_3/CNT. Fig. 1b presents the high-resolution scanning TEM (HR-STEM) image of a Pd-Cu alloy NP on the Pd_1Cu_3/CNTs. The HR-STEM image shows that the interplanar distances were 0.220 nm and presents two sets of (111) planes with an acute angle 70.5°. Fig. 1c is the STEM image of dispersed Pd-Cu alloy NP on the Pd_1Cu_3/CNT, and Fig. 1d–e presents the STEM-energy-dispersive X-ray spectroscopy (EDX) element mapping distributions of Pd and Cu, respectively. Based on the STEM-EDX elemental mapping, Cu and Pd are homogeneously distributed within the NPs. Fig. 1 indicates the alloying states of the nanocatalysts. The lattice parameters of fcc Pd and Cu metals are 0.226 and 0.208 nm, respectively, and the lattice parameters of the alloying NPs fall between these values.

Fig. 2 shows the XRD patterns of the Pd/CNTs, Pd_xCu_y/CNTs, and Cu/CNTs samples. The Pd/CNTs sample shows peaks at 40.1° (Pd(111)), 46.7° (Pd(200)), and 68.1° (Pd(220)), suggesting the synthesis of Pd NPs (JCPDS standard Pd 46-1043). The Cu/CNTs sample shows peaks at 43.3° (Cu(111)) and 50.4° (Cu(200)), indicating the synthesis of Cu NPs (JCPDS standard 04-0836(Cu)). The peaks located at ~42.8° for the Pd_1Cu_1/CNTs, Pd_3Cu_1/CNTs, and Pd/CNTs samples correspond to the C(101) reflection planes of carbon (JCPDS standard C 26-1077). Fig. 2b–d shows that the Pd peaks broaden and the 2θ angles increase from 40.1 to 41.4° as the Cu content increases, indicating that the Cu atoms have entered the Pd crystal to generate a fcc Pd-Cu alloy structure [12,13]. It should be noted that systems containing two or more metallic species may exist in several phases. The Pd_1Cu_3/CNTs show a perturbation peak at 41.3°, indicating that a PdCu intermetallic phase (JCPDS standard 48-1551 (CuPd)) may have formed within the Pd_1Cu_3/CNTs sample.

XPS was further utilized to examine the surface compositions and valence electronic structures of Pd_xCu_y/CNTs catalysts. Upon addition of Cu, the original Pd peak profile is gradually weakened (Fig. 3A). However, the preserved Pd 3d spectra of all the Pd_xCu_y/CNTs indicate that some Pd in monometallic phase remains dispersed on the catalyst surfaces. On the other hand, Fig. 3B shows a higher Cu^0 peak on the Pd_1Cu_3/CNTs than on the Cu/CNTs. Owing to the fact that more Cu (5.3 wt%) is present in Pd_1Cu_3/CNTs than in Cu/CNTs (3 wt%), we propose that the enhanced Cu^0 peak on Pd_1Cu_3/CNTs was caused by the spillover effect. In this process, the H_2 adsorbed on the noble metal surfaces decomposes to H atoms, and these dissociative H atoms migrate to alloyed metals or supporting oxides [14,15]. Accordingly, spill-over effects is known to exert significant influences in the field of

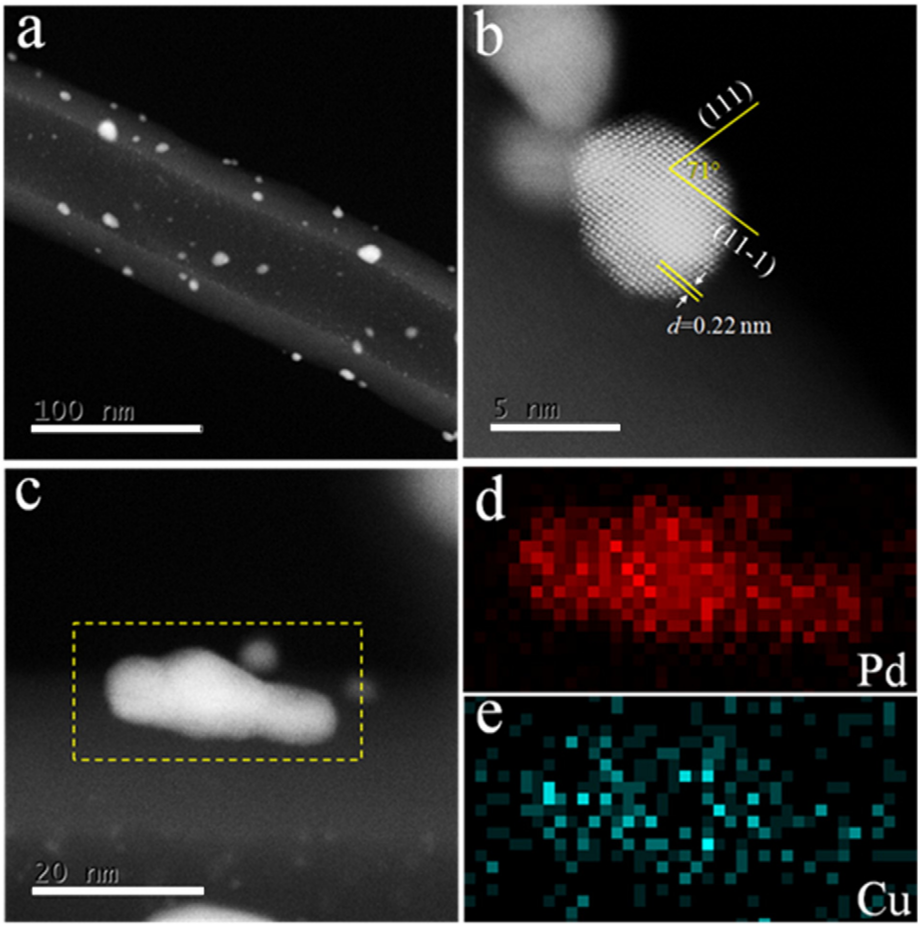

Fig. 1. (a) STEM image of Pd_1Cu_3/CNT. (b) HRTEM image of a Pd-Cu alloy NP on the Pd_1Cu_3/CNT. (c) STEM image of a dispersed Pd-Cu alloy NPs on the Pd_1Cu_3/CNT. (d) and (e) STEM-EDX element mapping distributions of Pd and Cu, respectively.